Capillarity ion concentration polarization for spontaneous biomolecular preconcentration mechanism

Yoonjee Oh,[1,a)] Hyomin Lee,[2,3,a)] Seok Young Son,[2] Sung Jae Kim,[2,4,5,b)] and Pilnam Kim[1,b)]

[1]*Department of Bio and Brain Engineering, Korea Advanced Institute of Science and Technology, 335 Gwahangno, Yuseong-gu, Daejeon 305-701, South Korea*
[2]*Department of Electrical and Computer Engineering, Seoul National University, 1 Gwanakro, Gwanakgu, Seoul 151-744, South Korea*
[3]*Institute of Advanced Machines and Design, Seoul National University, 1 Gwanakro, Gwanakgu, Seoul 151-744, South Korea*
[4]*Inter-University Semiconductor Research Center, Seoul National University, 1 Gwanak-ro, Gwanak-gu, Seoul 151-744, South Korea*
[5]*Big Data Institute, Seoul National University, 1 Gwanak-ro, Gwanak-gu, Seoul 151-742, South Korea*

(Received 15 October 2015; accepted 21 December 2015; published online 7 January 2016)

Ionic hydrogel-based ion concentration polarization devices have been demonstrated as platforms to study nanoscale ion transport and to develop engineering applications, such as protein preconcentration and ionic diodes/transistors. Using a microfluidic system composed of a perm-selective hydrogel, we demonstrated a micro/nanofluidic device for the preconcentration of biological samples using a new class of ion concentration polarization mechanism called "capillarity ion concentration polarization" (CICP). Instead of an external electrical voltage source, the capillary force of the perm-selective hydrogel spontaneously generated an ion depletion zone in a microfluidic channel by selectively absorbing counter-ions in a sample solution. We demonstrated a reasonable preconcentration factor (∼100-fold/min) using the CICP device. Although the efficiency was lower than that of conventional electrokinetic ICP operation due to the absence of a drift ion migration, this mechanism was free from the undesirable instability caused by a local amplified electric field inside the ion depletion zone so that the mechanism should be suitable especially for an application where the contents were electrically sensitive. Therefore, this simple system would provide a point-of-care diagnostic device for which the sample volume is limited and a simplified sample handling is demanded. © *2016 AIP Publishing LLC*. [http://dx.doi.org/10.1063/1.4939434]

I. INTRODUCTION

The ability to control ion transport through a nanoporous membrane or nanochannel via an external electric field has been utilized for significant engineering applications, such as electrodesalination,[1–4] concentrating biomolecules,[5–9] separation,[10,11] fluid pumping and switching,[12] nanofluidic diodes, and ionic field effect transistors.[13–17] Elucidating the fundamentals of ion transportation also remains an active research area because various related phenomena are not fully understood yet. Ion concentration polarization (ICP) is a representative phenomenon of such novel ion transport in a nanoscale fluidic device, usually driven by an external electric field.[5,18] For a cation-selective membrane under dc bias, the typical behavior is that the ion concentration at the anodic side becomes largely depleted, while the concentration at the cathodic side is enriched.[18–20]

[a)]Y. Oh and H. Lee contributed equally to this work.
[b)]Authors to whom correspondence should be addressed. Electronic addresses: gates@snu.ac.kr and pkim@kaist.ac.kr

The movement of ions through a nanoporous material can be driven by three different types of motion: a drift motion due to an electric potential gradient, a diffusive motion due to a concentration gradient, and an electro-convective motion due to fluid motion.[18,21,22] In electrically driven ICP, the local electrical field inside the zone is significantly amplified due to the extremely low ion concentration inside the depletion zone (or ICP zone), so that the local electrical resistance inside the zone increases significantly, more than 10 times compared to one outside the zone.[18,23] Thus, undesirable ultra-fast vortical fluid motions are induced inside the zone, and the zone of high electrical resistance is continuously expanded; thus, the motions are directly correlated with undesirable instability and low power efficiency, which become a serious nuisance for stable ICP device operation.[23–29]

Nonetheless, ICP has been used for several novel engineering applications because of the ability to maintain an extremely low concentration inside the ICP zone at the anodic side with a cation-selective membrane. For example, the electro-neutrality of extremely low ionic concentrations inside the ion depletion zone can be used to reject for most charged species to enter the zone, allowing charged molecules to accumulate at the boundary of the ion depletion zone with the proper aid of a tangential field (either pressure or electrical, or both) through the zone.[5,30–32] The mechanism has been used directly to preconcentrate proteins with a high amplification ratio and has drawn significant attention in portable biological sample preparation methods.

Here, we present a new ICP device in which the ICP is spontaneously driven without an external electric bias; thus, there is no local amplified electric field inside the ion depletion zone.[12] The experimental micro-/nanofluidic device consists of a perm-selective ionic hydrogel shown in Figure 1. Ionic hydrogel has extensively utilized as a perm-selective material for ICP operation in various literature.[33–40] Using this system, the capillary force (or capillarity) of the perm-selective nanoporous hydrogel instead of an electric bias drove the fluid into the hydrogel matrix, while its co-ions in the fluid were rejected to enter the hydrogel. This new kind of ICP

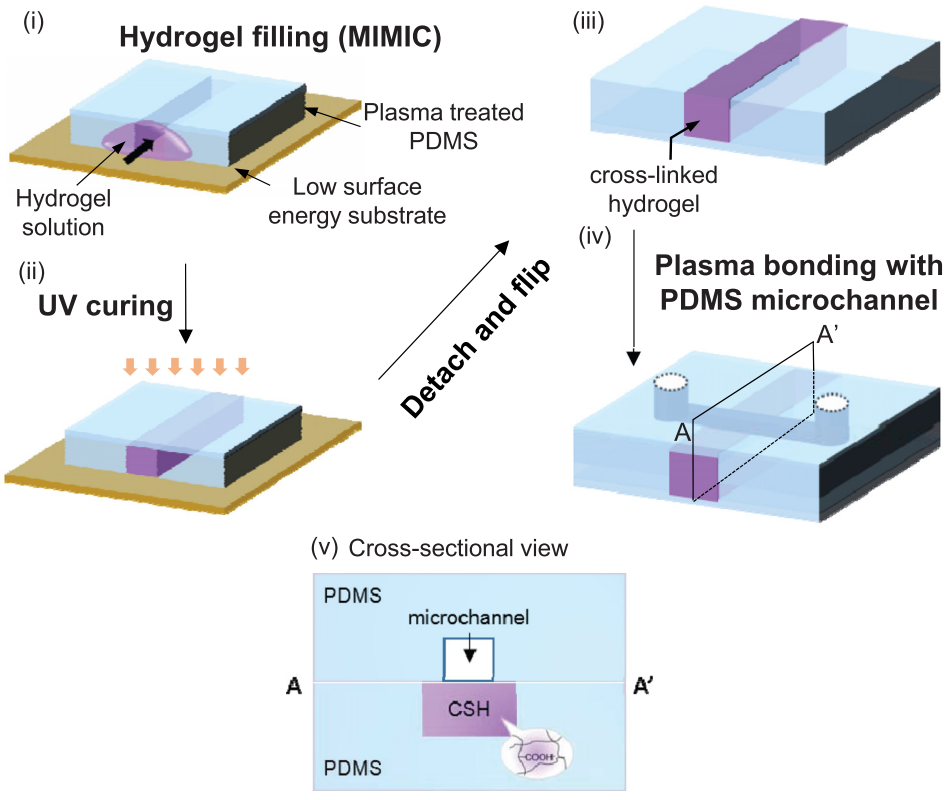

FIG. 1. Fabrication processes of ionic hydrogel embedded PDMS substrate by hydrophobic surface modification and micromolding in capillaries (MIMIC).

was named as Capillarity ICP (CICP). Biomolecular preconcentration was demonstrated using CICP mechanism at 100-fold preconcentration factor. While the total process time was longer than one with the electrokinetically driven ICP mechanism, the method permitted the same ICP phenomenon to be obtained without amplified vortical fluid motion or electrokinetic instability, which do not exist at all in this system. Additionally, this CICP mechanism can be maintained for an adjustable duration by controlling the dimensions of the nanoporous network (i.e., its capillarity).

II. EXPERIMEMTAL SECTION

A. Materials

Polydimethylsiloxane (PDMS) elastomer composed of prepolymer and curing agent was purchased from Dow Corning (Sylgard 184). Green Fluorescent Protein (GFP) was purchased from CloneTech. Fluorescent polystyrene particles of 500 nm diameter (Invitrogen) were used for tracking the fluid motions. For cationic selective hydrogel (CSH), we used a precursor mixture of ionic-monomer, 4-hydroxybutylacrylate (4-HBA) and acrylic acid (AA) in a weight ratio of 8.5:1.1. These materials were purchased from Sigma-Aldrich and vacuum-distilled prior to use.

B. Fabrication of nanoporous-junctions device

To cure the PDMS prepolymer, a mixture of 10:1 silicone elastomer and curing agent was poured onto the silicon masters prepared by photolithography and placed at 60 °C for 2 h. The masters had protruding features with the impression of microfluidic channels (50–100 μm in width and 10 μm in height). The masters used for hydrogel junctions had 10–350 μm in width and 15 μm in depth. After curing, PDMS molds were cleanly detached from the masters. To fabricate a perm-selective nanoporous junction, we used negatively charged hydrogel in the form of a mixture of 4-HBA and AA.[33] The perm-selective hydrogel was filled inside a single channel on the PDMS layer by spontaneous capillarity-driven flow, which was originally developed in a technique called "micromolding in capillaries (MIMIC)"[41] (Figure 1). After placing a PDMS channel mold onto silane (octadecyltrichlorosilane, OTS) treated silicon wafer, the hydrogel precursor was pulled inside the microchannel by spontaneous capillarity-driven flow and subsequently exposed to UV light (10 mW/cm^2) for 10 s for photo-crosslinking. For a strong bonding between hydrogel and PDMS surface, we treated the PDMS surface with oxygen plasma prior to introducing the hydrogel precursor, which turned out to be important to prevent swelling and subsequent detachment of the hydrogel. Then, the microfluidic PDMS channel (top) and the ionic-hydrogel embedded PDMS substrate (bottom) were irreversibly bonded by oxygen plasma treatment for 60 s (Cute-MP, Femto Science, Korea). As a consequence, the volume changes that are created from a swelling behavior of hydrogel can be excluded in our system, as evidenced by robust channel bonding without any leakage along the microchannel near the hydrogel junction when a positive pressure was applied from a reservoir. Furthermore, the nanoporous-junction device presented here allows for direct observation of the ion-exchange phenomena through the charged nanopores without any physical disturbances along the microchannel. This feature was not possible with previous approaches, as the liquid flow was typically interrupted in the presence of a constructed hydrogel plug inside the main channel.[42,43] In our approach, the ionic hydrogel exhibits a fixed charge inside matrix, owing to the deprotonation of acid-groups.[44,45] The ionic property of the groups plays a deterministic role of cationic perm-selectivity of nanopores.

C. Experimental process

To confirm the functionality of hydrogel pads in detail, we visualized the ion depletion/enrichment zone by tracking a GFP and fluorescent microspheres with external electric fields. 1 mM dibasic sodium phosphate at $p\mathrm{H} = 7.5$ as a main buffer solution was used. All the flow motions and ion transport were imaged under an inverted fluorescence microscope (Olympus,

IX-51) with CCD camera. Sequences of images were analyzed by ImageJ. A dc power supplier (Keithley 238) was used in case of electrically driven ICP to apply electrical potential to each reservoir and to measure the ionic current through either the hydrogel junction or single microchannel. An external pressure field, if needed, was applied by either syringe pump (Harvard apparatus, PHD2000) or gravitational force (level differences between reservoirs). To investigate the capillarity driven ICP phenomena, the same experimental methods (fluorescent tracking, visualization, etc.) were used except the external power source.

III. RESULTS AND DISCUSSION

A. Capillarity-driven ICP phenomena through an ionic hydrogel

ICP is a novel ion transport phenomenon, typically driven by an external electric field through a perm-selective nanoporous membrane, which produces a depleted and enriched ionic concentration at the anode and cathode, respectively.[5,30–32] The ion movement through the membrane is driven mainly by three types of motion. The first is drift motion due to an electric potential gradient ($\mathbf{j_i^{drift}} = -\mu_E z_i \nabla\phi c_i$ where v_i and z_i are the mobility and valence of the ith ion, F is the Faraday number, ϕ an electrical potential, and c_i, bulk electrolyte concentration). The second, diffusion motion, is due to an ion concentration gradient ($\mathbf{j_i^{diff}} = -D_i \nabla c_i$, where D_i is the diffusivity of the ith ions) and the third is convective motion due to a fluid motion ($\mathbf{j_i^{conv}} = c_i \mathbf{v}$, where $\mathbf{v}$ is the bulk convection).[5,30–32] Thus, Nernst-Planck equation for describing ion flux for an electrokinetic ICP system would be $\partial c_\pm/\partial t = -\nabla \cdot (-D_\pm \nabla c_\pm \mp c_\pm \mu_E \nabla\phi + c_\pm \mathbf{v})$.

While electrokinetic ICP utilizes an electrical bias as the main driving force to initiate the ICP zone, one can employ an alternative driving force; in this work, the spontaneous imbibition of liquids by a capillary force through an ionic nanoporous hydrogel was used. Indeed, the hydrogel pad was able to absorb the liquid in the microchannel to create a bulk flow as illustrated in Figure 2(a). During the continuous imbibition, water with only cation is absorbed vertically into the CSH pad, leaving an ICP zone on the pad, which is identical to an electrokinetically driven ICP. To confirm the capillarity-driven bulk flow, we injected negatively charged fluorescent microparticles in the microfluidic channel. Our observation indicated that particles suspended in the liquid converged toward the hydrogel pad from both reservoirs as shown in Figure 2(a) (see the supplementary video SV1).[60] This showed that the liquid was absorbed into the pad and the calculated flow rate was ~0.15 nl/min. When neutral water molecules are transported into the hydrogel pad, only dissolved counter-ions (cations in this case) can go through the pad because the pad retained its perm-selectivity. Here this perm-selectivity of the ionic hydrogel was pre-confirmed by electrokinetic ICP operation[33] (see the supplementary material).[60] As long as the pad can absorb the liquid, both positively and negatively charged species are accumulated on the hydrogel pad, especially at both the left-top and right-top corner of the microchannel as shown in Figure 2(b). This was because the CICP zone created on the hydrogel pushed both polarities of species away from the hydrogel. Unlike the continuous expansion of electrokinetic ICP layer, CICP layer was incapable of such expansion due to slow imbibition so that the charged species stayed on the hydrogel pad. Due to the auto-fluorescence of the hydrogel pad, the preconcentration factor on the pad could not be measured. Thus, after 1 min of operation, an external pressure field was applied by tipping a reservoir so that the accumulated sample (GFP) was able to escape from the hydrogel area, as shown in Figure 2(c) (see the supplementary video SV2).[60] GFP was squeezed from the top and bottom corners of the microchannel which was the top-right and the top-left corner in the schematics shown in Figure 2(b). Thus, squeezing from the top and bottom in Figure 2(c) provided a critical evidence of the formation of ICP layer. Compared with electrically driven ICP operation, which produces a preconcentration factor of more than 1000 fold in a minute, the preconcentration factor was only 100 fold in the CICP, because the mechanism does not involve the drift (electrical) transport of ions. However, this method can be significantly useful for, for example, point of care systems, where external electricity is not always available or the stress-free preconcentration of the cell is required to avoid the disruption of the living-cell membrane.

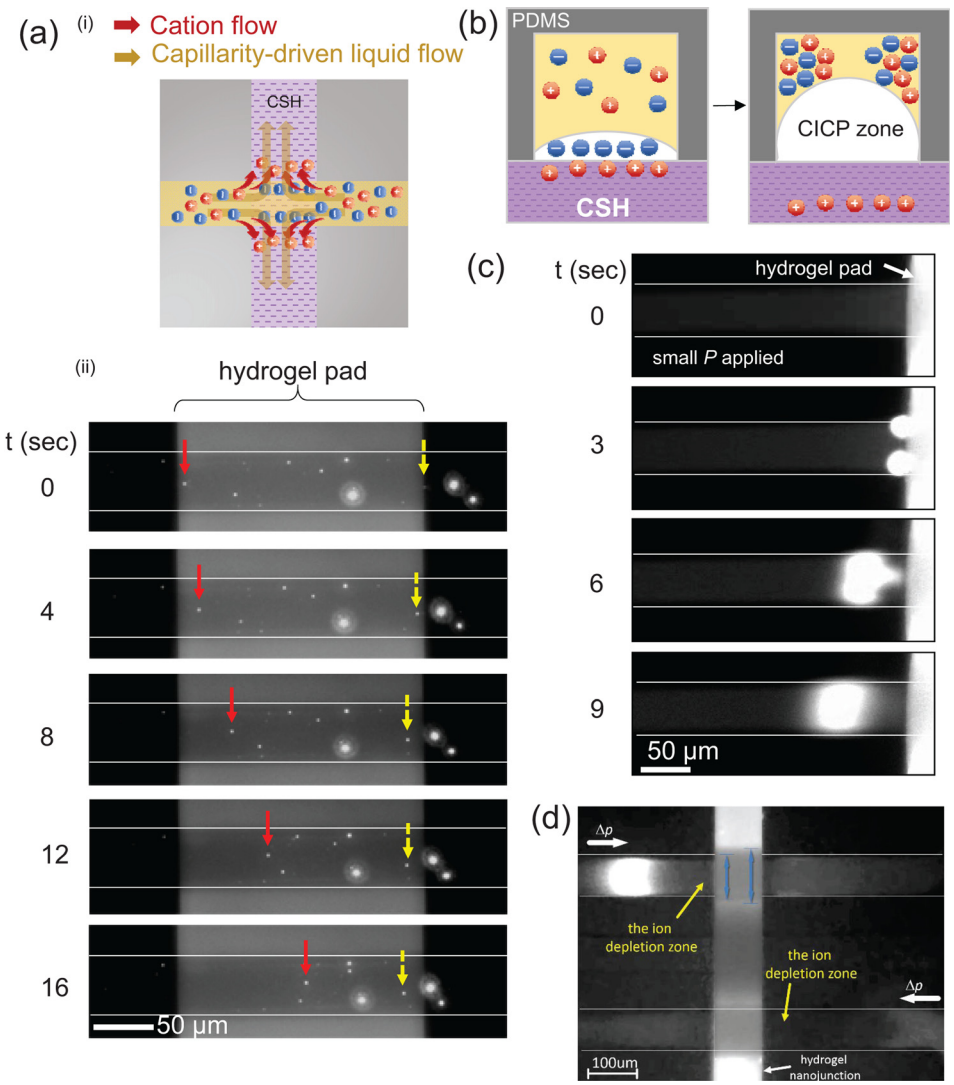

FIG. 2. (a) An illustration of ion movements and the mechanism of capillarity driven ICP phenomena inside microchannels and its experimental demonstration of fluorescent particle tracking near the hydrogel pad. Particles from both ends of the microchannel converged into the hydrogel pad due to the capillarity of the pad. The absorption continued for more than 30 min depending on the geometry of the pad. (b) Schematic diagram of preconcentrated molecules in top-left and top-right corners of microchannel. (cross-sectional view). (c) Concentrated GFPs on the hydrogel after 1 min of capillarity driven ICP. They were coming from the top and bottom of the microchannel as illustrated in (b). (d) The formation of the ion depletion zone in the direction against the external flow coming in.

In addition to this experiment that did not involve a tangential field, we applied a flow rate by the liquid level difference between reservoirs. The rate was measured to be the same as the capillarity-driven liquid flow (∼0.15 nl/min) during the process. Fluorescent samples were injected into both microchannels, which were physically separated, and the depletion zones were formed immediately in both microchannels as shown in Figure 2(d). Eye-catching features in the Figure 2(d) (also see the supplementary video SV3)[60] were that the zones were formed in the direction against the external pressure field (from left hand side in the upper channel and from right hand side in the lower channel). This was because an electrostatic force was able to repel the GFP so that the injected GFP was incapable of passing the depletion zone and accumulated at a virtual boundary where the drag force and the repulsion force were balanced. It has been called the ion depletion zone (black region from the hydrogel to the boundary) and this was identical to the ion depletion zone by the conventional ICP operation that had been

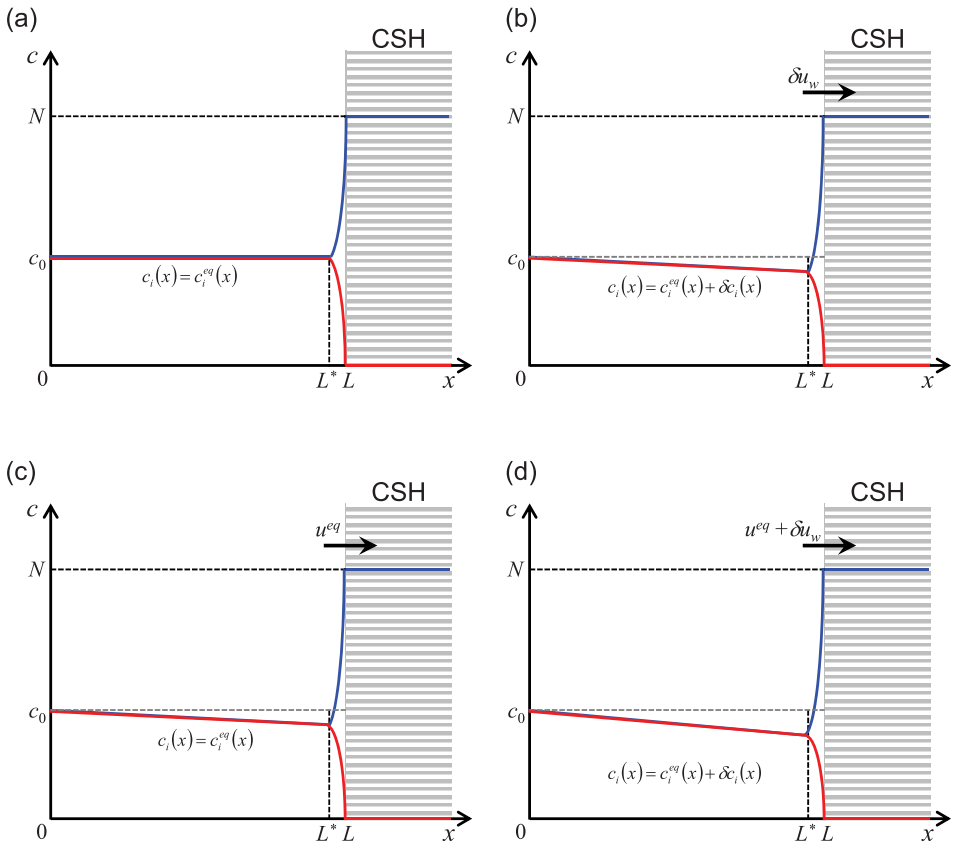

FIG. 3. Schematic plots of concentration profiles for both cation and anion inside CICP layer (a) at the thermal equilibrium (initial state), (b) with the infinitesimal variation of imbibition rate, (c) at new equilibrium state, and (d) with the infinitesimal variation of imbibition rate after the new equilibrium state.

observed in a number of literature.[5,18,20,29,46,47] If there was not such repulsive force, all GFP sample should just flow through toward each reservoir.

While the ion enrichment zone was formed at the cathodic side of microchannel in the conventional ICP operation, the enrichment zone was not observed in the CICP operation. This was because the counter-ions were slowly penetrated into the hydrogel pad in CICP operation, while they quickly passed across nanochannel by aid of external electric field and formed the enrichment zone in a cathodic microchannel in the conventional ICP operation. This was also confirmed that the blue arrows on the hydrogel pad indicated the penetration length of water with counter-ions in Figure 2(d). The counter-ions were not "passed," but "passing" across the nanoporous hydrogel in CICP operation.

B. Local electroneutrality of diffuse layer during the development of CICP layer

In an electrokinetic ICP, it has been known that local electroneutrality is satisfied for the diffuse layer (i.e., a region except the electric double layer (EDL) of perm-selective nanoporous membrane and the space charge layer).[48–53] While only cation passed through the cation selective membrane under external electric field, anion moved to the reservoir. Thus, local electroneutrality of diffuse layer retained. In a CICP process, it seemed that the local electroneutrality should be broken due to the absence of the external electric field by observing anions were accumulated further at the interface between the diffuse layer and the EDL. The accumulation would result in local inversion of polarity at the interface (i.e., positive polarity inside EDL and negative polarity outside EDL). However, this was impossible in a physical sense. In order to

resolve the unrealistic situation, we suggested the following theoretical justifications for the electroneutrality during CICP process.

First, consider the equilibrium state as shown in Figure 3(a). In the figure, cation (blue) and anion (red) formed the EDL in $L^* \leq x \leq L$ where electroneutrality was broken, while the diffuse layer in $0 \leq x < L^*$ was electroneutral.[54–56] If there was the infinitesimal variation of flow (δu_w) through CSH, the flow would cause the variation of cation concentration (δc_+) as shown in Figure 3(b). The mathematical form about the small variation of cationic flux (δj_+) was

$$\delta j_+ = -D\frac{\mathrm{d}\delta c_+}{\mathrm{d}x} + \mu_E c^{eq}\delta E + c^{eq}\delta u_w + O(\delta c \delta u_w) \text{ in } 0 \leq x < L^*, \tag{1}$$

where D is the diffusivity, μ_E is the electrophoretic mobility, c^{eq} is equilibrium concentration of diffuse layer, and δE is the small variation of imbibition-induced electric field. For the simplicity, we assumed the same diffusivity and electrophoretic mobility of cation and anion. At the equilibrium state, cation concentration and anion concentration inside the diffuse layer ($0 \leq x < L^*$) should be the same because of electroneutrality, so that the equilibrium concentration of both ionic species was able to denote as c^{eq} ($=c_0$). Since the variation of flow was infinitesimally small, the concentration gradient would be neglected so that Equation (1) became

$$\delta j_+ \approx \mu_E c^{eq}\delta E + c^{eq}\delta u_w. \tag{2}$$

When the hydrogel was assumed to be an ideal cation selective membrane, the cation concentration inside the membrane was equal to the Donnan concentration (N) which should be larger than the reservoir concentration (c_0) and anion concentration was zero.[7] Hence, cationic flux through the hydrogel was

$$\delta j_+ = N\delta u_w. \tag{3}$$

Using Equations (2) and (3), the following relation was obtained:

$$\mu_E c^{eq}\delta E = (N - c^{eq})\delta u_w \approx N\delta u_w. \tag{4}$$

The last equality in the above equation came from the assumption of ideal selective membrane ($N \gg c_0 = c^{eq}$). Meanwhile, the variation of anionic flux was

$$\delta j_- \approx -\mu_E c^{eq}\delta E + c^{eq}\delta u_w. \tag{5}$$

Substituting Equation (4) into Equation (5) yielded

$$\delta j_- = -(N - c^{eq})\delta u_w \approx -N\delta u_w. \tag{6}$$

Using Equation (3), following was held:

$$\delta j_- = -\delta j_+. \tag{7}$$

Equation (7) meant that the magnitude of anionic flux was equal to that of cationic flux but the direction was counter to cationic flux in the case of the absence of external electric field. Since the anionic flux through the hydrogel was zero, anion concentration should be depleted until the local electroneutrality was satisfied. Therefore, local electroneutrality inside the diffuse layer would be held at the trigger stage during developing CICP layer and the above fluxes led to new equilibrium layer as shown in Figure 3(c). In the new equilibrium, there was non-zero equilibrium velocity (u^{eq}) so that another variational analysis should be conducted to verify the local electroneutrality of the diffuse layer as shown in Figure 3(d). In the range of $0 \leq x < L^*$ as our region of interest, the equilibrium flux of each ionic species was denoted as

$$j_+^{eq} = -D\frac{\mathrm{d}c^{eq}}{\mathrm{d}x} + \mu_E c^{eq}E^{eq} + c^{eq}u^{eq} = Nu^{eq}, \tag{8}$$

and

$$j_-^{eq} = -D\frac{\mathrm{d}c^{eq}}{\mathrm{d}x} - \mu_E c^{eq}E^{eq} + c^{eq}u^{eq} = 0, \tag{9}$$

in which $c_+^{eq} = c_-^{eq} = c^{eq}$ was held by the verification through Equations (1)–(7). Subtracting Equation (9) from Equation (8), the equilibrium electric field was

$$E^{eq} = \frac{Nu^{eq}}{2\mu_E c^{eq}}. \tag{10}$$

The variation of cationic flux due to infinitesimally small δu_w with neglecting diffusion term was

$$\delta j_+ \approx \mu_E \delta c_+ E^{eq} + \mu_E c^{eq}\delta E + \delta c_+ u^{eq} + c^{eq}\delta u_w = N\delta u_w. \tag{11}$$

Using the relation of $N \gg c_0 \geq c^{eq}$

$$\delta E = \frac{N}{\mu_E c^{eq}}\left(\delta u_w - \frac{u^{eq}\delta c_+}{2c^{eq}}\right). \tag{12}$$

The variation of anionic flux with neglecting diffusion term was

$$\delta j_- \approx -\mu_E \delta c_- E^{eq} - \mu_E c^{eq}\delta E + \delta c_- u^{eq} + c^{eq}\delta u_w. \tag{13}$$

Substituting Equation (12) into Equation (13) and using the relation of $N \gg c_0 \geq c^{eq}$

$$\delta j_- \approx \frac{(\delta c_+ - \delta c_-)N}{2c^{eq}}u^{eq} + \delta c_- u^{eq} - N\delta u_w. \tag{14}$$

Through the scaling analysis, following inequalities were obtained:

$$O\left(\frac{\delta c_i N}{c^{eq}}\right),\ O(\delta c_i) \ll O(N), \tag{15}$$

and thus

$$\delta j_- \approx -N\delta u_w = -\delta j_+. \tag{16}$$

Therefore, we concluded that the local electroneutrality inside the diffuse layer would be held during developing CICP layer.

C. Capillarity-driven ICP versus physical filtration

To distinguish this process from regular physical filtration, such as ultra-filtration, we continuously applied an external pressure field (Q_{ext} of 0.15 nl/min) using different liquid levels in the reservoirs (the schematics were shown in the inset of Figure 4(a)) during operation. Because the volume of liquid into the hydrogel pad of 20 μm width was relatively low, neither the ion depletion zone nor pre-concentrated GFPs were observed, as shown in the first column of Figure 4(a). However, increasing the width of the hydrogel pad (i.e., increased volume of penetrated liquid) allowed the formation of the ion depletion zone, as observed in the comparison of 50 μm and 100 μm widths, shown the second and third column in Figure 4(a).

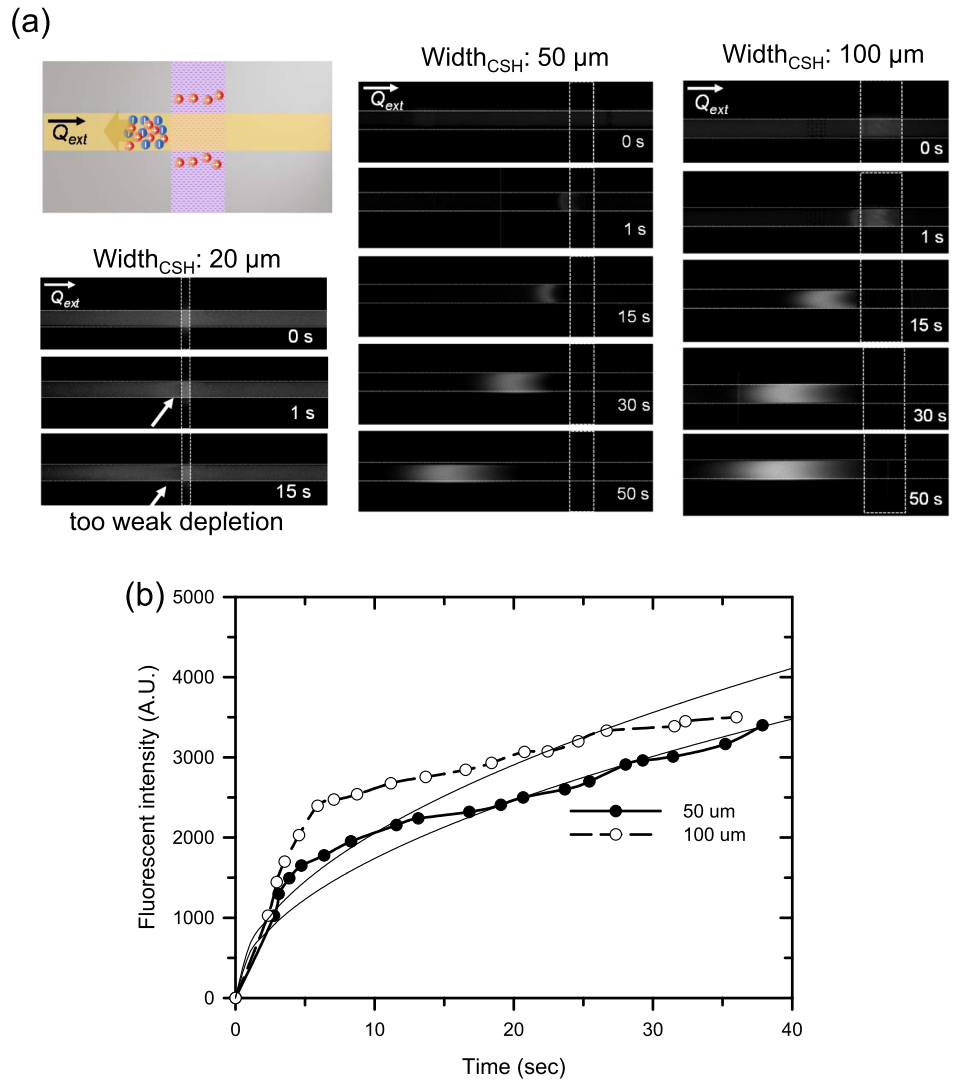

FIG. 4. (a) Ion exclusion operation using the CICP with continuous tangential pressure fields with the widths of hydrogel at 20 μm, 50 μm, and 100 μm. The external pressure was applied to the microchannel using liquid level differences between reservoirs. The concentrated plugs were formed against the external pressure field showing one can differentiate this repulsive operation from physical filtration. (b) The sample was concentrated faster with wider hydrogel pad (which had stronger capillarity).

If this operation were a "typical" physical filtration, with liquid absorbing into the hydrogel, the accumulated sample should flow along the pressure field (left to right in this case). However, the accumulated plug was formed and moved (or migrated) against the direction of flow coming in (toward the left-hand side of the hydrogel pad), and the fluorescent intensity of the accumulated sample increased as a function of time, as shown in Figure 4(b). This showed that the fluorescent intensity of the concentrated GFPs rapidly increased with a wider hydrogel pad, as compared with a narrower pad. The increase in intensity was roughly proportional to the square root of time (the two solid lines in Figure 4(b)); thus $V = ASt^{1/2}$, where V is a liquid volume absorbed into a porous medium and A and S are the cross-sectional area and the porosity of the porous medium, respectively. However, the actual florescent intensity was saturated because of the limited water-absorbing efficiency of the hydrogel pad. Thus, sample trapping should originate from electrostatic repulsion, which was essentially similar to an electrokinetic ICP preconcentration mechanism. This mechanism also differs from the formation of a solute-

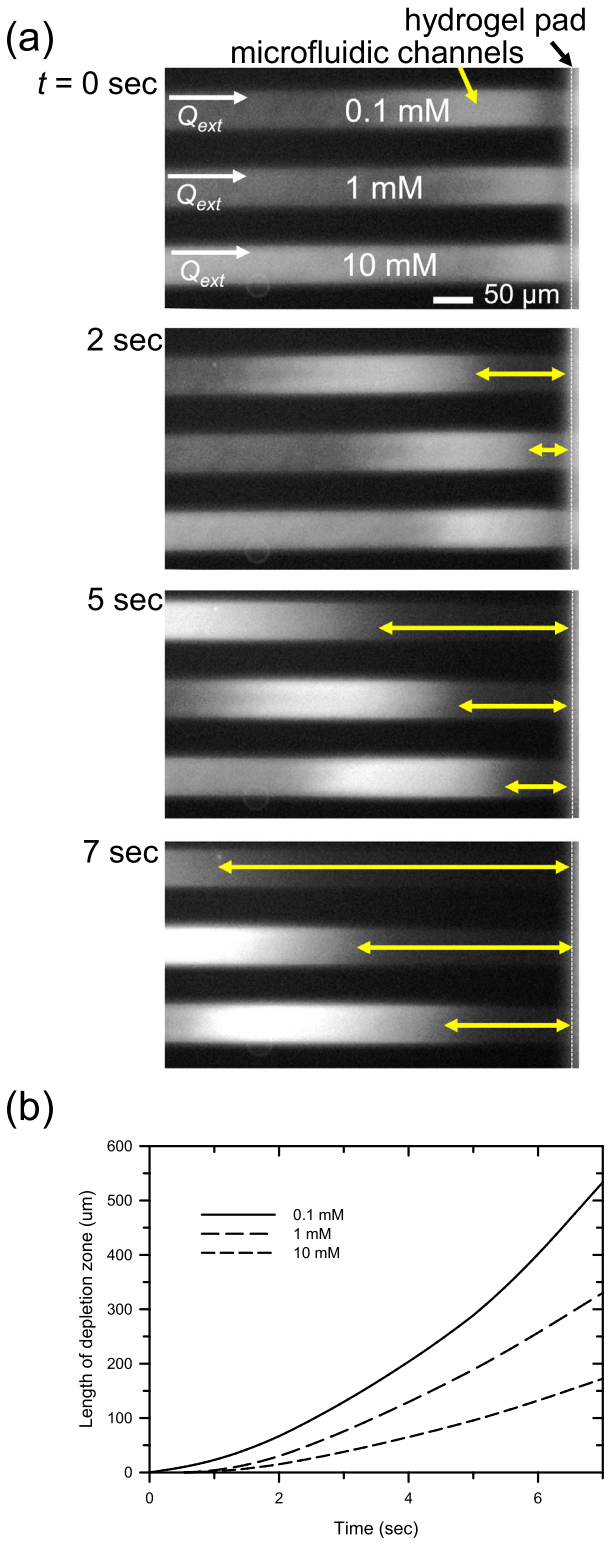

FIG. 5. The effect of buffer concentration to the propagation velocity of the ion depletion zone. Since a lower buffer concentration provides severe perm-selectivity, the propagation velocity of the ion depletion zone was faster at low buffer concentration. The external flow rate was controlled by syringe pump. The flow rate was similar to the capillarity-driven liquid flow (~0.15 nl/min) during the process. The results also showed that the capillarity driven ICP was based on an electrorepulsive mechanism, not physical filtration.

free zone due to surface charge-based forces.[57,58] Although this exclusion had occurred near metal-water or Nafion-water interfaces, our mechanism involves the infiltration of water through the nanopores, with the ion depletion zone remaining near the interface which has not been observed in surface charge based exclusion.

D. Bulk electrolyte concentration dependency of CICP

Further evidence confirming the CICP mechanism includes the buffer concentration dependency. Because the conductivity of the bulk electrolyte plays a critical role in determining the extent of perm-selectivity,[47] the characteristics of ICP should depend on the bulk electrolyte concentration. Simply, since the thickness of electrical double layer is inversely proportional to the square root of bulk electrolyte concentration, a lower electrolyte concentration should retain a thicker electrical double layer so that the ion depletion zone propagated more (i.e., higher perm-selectivity with lower electrolyte concentration). In contrast, normal physical filtration should be independent of the buffer concentration. Here we demonstrated that the observed CICP mechanism was highly dependent on the buffer concentration. Three isolated microchannels were filled with buffer samples having three different concentrations (0.1 mM, 1 mM, and 10 mM of dibasic sodium phosphate), and the propagation velocities of the ion depletion zone against the external pressure field were measured, as shown in Figure 5. In this experiment, Q_{ext}s were applied by syringe pump and the rate was 0.15 nl/min. Because a lower electrolyte concentration provides strong perm-selectivity,[18,20,47,59] the propagation velocity of the ion depletion zone was higher with a lower buffer concentration. Because a higher perm-selective ion transport demanded a faster mismatch of ion concentration near the nanopore, the propagation speed of the ICP zone should be faster at lower bulk concentration, as shown in Figure 5. These observations indicated that the capillary force of the ionic nanoporous hydrogel could drive perm-selective ion transport with no external electric bias.

IV. CONCLUSION

In this work, we demonstrated biomolecular preconcentration using CICP mechanism. By utilizing nanoporous (perm-selective) hydrogel, the entering co-ions were rejected while spontaneous imbibition through the hydrogel. This ion imbalance initiated the formation of the ion depletion zone and the zone acted as an electrical filter like the conventional electrokinetic driven ICP process. During the development of CICP layer, the local electroneutrality was satisfied as we theoretically proved. The difference between the physical filtration and the electrostatic rejection was confirmed by either applying a tangential pressure field (the preconcentrated plugs were formed in the direction against the flow coming in) or measuring the propagation velocities of the ion depletion zone (lower bulk concentration had higher propagation velocity).

All forms of typical ICP operation involved an electrical source, producing undesirable instability issues due to a local amplified electric field inside the ion depletion zone[12,23,28,33] which was a major problem for reliable and long-term stable operation. Because the CICP mechanism does not involve any electrical power source, it offered significant advantages in terms of power consumption and stable operation compared with the conventional electrokinetic ICP mechanism. In addition, the CICP mechanism was highly suitable for analysis of an electrically sensitive analyte, such as cells with weak cell membrane. However, compared with electrically driven ICP operation, which has a preconcentration factor of more than 1000 fold in a minute, the factor was only 100 fold in CICP operation because the scheme did not involve the drift (electrical) transport of ions.

ACKNOWLEDGMENTS

The authors gratefully acknowledge helpful discussions with and the support of Professor Jongyoon Han at Massachusetts Institute of Technology. P. Kim and Y. Oh acknowledge the support of the National Research Foundation (NRF) of Korea (NRF-2011-35B-D00013). S. J. Kim,

H. Lee and S. Y. Son acknowledge the support of the NRF (No. 2013R1A1A1008125 and No. 2014-048162) and BK21 plus program of Creative Research Engineer Development IT, Seoul National University.

[1]S. J. Kim, S. H. Ko, K. H. Kang, and J. Han, Nat. Nanotechnol. **5**, 297–301 (2010).
[2]R. Kwak, S. J. Kim, and J. Han, Anal. Chem. **83**, 7348–7355 (2011).
[3]R. Kwak, G. F. Guan, W. K. Peng, and J. Y. Han, Desalination **308**, 138–146 (2013).
[4]A. Subramani, M. Badruzzaman, J. Oppenheimer, and J. G. Jacangelo, Water Res. **45**, 1907–1920 (2011).
[5]S. J. Kim, Y.-A. Song, and J. Han, Chem. Soc. Rev. **39**, 912–922 (2010).
[6]Y. C. Wang and J. Y. Han, Lab Chip **8**, 392–394 (2008).
[7]R. B. Schoch, J. Han, and P. Renaud, Rev. Mod. Phys. **80**, 839–883 (2008).
[8]D. Hlushkou, R. Dhopeshwarkar, R. M. Crooks, and U. Tallarek, Lab Chip **8**, 1153–1162 (2008).
[9]J. Choi, K. Huh, D. J. Moon, H. Lee, S. Y. Son, K. Kim, H. C. Kim, J.-H. Chae, G. Y. Sung, H.-Y. Kim, J. W. Hong, and S. J. Kim, RSC Adv. **5**, 66178–66184 (2015).
[10]K. Schmidt-Rohr and Q. Chen, Nat. Mater. **7**, 75–83 (2008).
[11]S. R. Liu, Q. S. Pu, L. Gao, C. Korzeniewski, and C. Matzke, Nano Lett. **5**, 1389–1393 (2005).
[12]S. J. Kim, L. Li, and J. Han, Langmuir **25**, 7759–7765 (2009).
[13]I. Vlassiouk and Z. S. Siwy, Nano Lett. **7**, 552–556 (2007).
[14]H. Daiguji, Y. Oka, and K. Shirono, Nano Lett. **5**, 2274–2280 (2005).
[15]R. Karnik, R. Fan, M. Yue, D. Y. Li, P. D. Yang, and A. Majumdar, Nano Lett. **5**, 943–948 (2005).
[16]B. Kim, J. Heo, H. J. Kwon, S. J. Cho, J. Han, S. J. Kim, and G. Lim, ACS Nano **7**, 740–747 (2013).
[17]S.-H. Lee, H. Lee, T. Jin, S. Park, B. J. Yoon, G. Y. Sung, K.-B. Kim, and S. J. Kim, Nanoscale **7**, 936–946 (2015).
[18]S. J. Kim, Y.-C. Wang, J. H. Lee, H. Jang, and J. Han, Phys. Rev. Lett. **99**, 044501 (2007).
[19]I. H. Shin, K.-j. Kim, J. Kim, H. C. Kim, and H. Chun, Lab Chip **14**, 1811–1815 (2014).
[20]Q. Pu, J. Yun, H. Temkin, and S. Liu, Nano Lett. **4**, 1099–1103 (2004).
[21]R. F. Probstein, *Physicochemical Hydrodynamics: An Introduction* (Wiley-Interscience, 1994).
[22]S. M. Rubinstein, G. Manukyan, A. Staicu, I. Rubinstein, B. Zaltzman, R. G. H. Lammertink, F. Mugele, and M. Wessling, Phys. Rev. Lett. **101**, 236101 (2008).
[23]S. J. Kim, S. H. Ko, R. Kwak, J. D. Posner, K. H. Kang, and J. Han, Nanoscale **4**, 7406–7410 (2012).
[24]I. Rubinstein and B. Zaltzman, Phys. Rev. E **72**, 011505 (2005).
[25]H. C. Chang, G. Yossifon, and E. A. Demekhin, in *Annual Review of Fluid Mechanics*, edited by S. H. Davis and P. Moin (Annual Reviews, Palo Alto, 2012), Vol. 44, pp. 401–426.
[26]G. Yossifon and H. C. Chang, Phys. Rev. E **81**, 066317 (2010).
[27]G. Yossifon, P. Mushenheim, Y. C. Chang, and H. C. Chang, Phys. Rev. E **81**, 046301 (2010).
[28]I. Cho, G. Sung, and S. J. Kim, Nanoscale **6**, 4620–4626 (2014).
[29]S. Nam, I. Cho, J. Heo, G. Lim, M. Z. Bazant, D. J. Moon, G. Y. Sung, and S. J. Kim, Phys. Rev. Lett. **114**, 114501 (2015).
[30]C. H. Chen, A. Sarkar, Y. A. Song, M. A. Miller, S. J. Kim, L. G. Griffith, D. A. Lauffenburger, and J. Han, J. Am. Chem. Soc. **133**, 10368–10371 (2011).
[31]S. H. Ko, Y. A. Song, S. J. Kim, M. Kim, J. Han, and K. H. Kang, Lab Chip **12**, 4472–4482 (2012).
[32]S. H. Ko, S. J. Kim, L. Cheow, L. D. Li, K. H. Kang, and J. Han, Lab Chip **11**, 1351–1358 (2011).
[33]P. Kim, S. J. Kim, K.-Y. Suh, and J. Han, Nano Lett. **10**, 16–23 (2010).
[34]H. G. Chun, T. D. Chung, and J. M. Ramsey, Anal. Chem. **82**, 6287–6292 (2010).
[35]C. Duan, W. Wang, and Q. Xie, Biomicrofluidics **7**, 026501 (2013).
[36]M. Kim and T. Kim, Analyst **138**, 6007–6015 (2013).
[37]M. Kim and T. Kim, Sens. Actuators, B **202**, 1229–1236 (2014).
[38]C.-L. Chen and R.-J. Yang, Electrophoresis **33**, 751–757 (2012).
[39]J.-y. Wang, Z. Xu, Y.-k. Li, C. Liu, J.-s. Liu, L. Chen, L.-q. Du, and L.-d. Wang, Appl. Phys. Lett. **103**, 043103 (2013).
[40]H. Kim, J. Kim, E.-G. Kim, A. J. Heinz, S. Kwon, and H. Chun, Biomicrofluidics **4**, 043014 (2010).
[41]Y. N. Xia, E. Kim, and G. M. Whitesides, Chem. Mater. **8**, 1558–1567 (1996).
[42]R. Dhopeshwarkar, R. M. Crooks, D. Hlushkou, and U. Tallarek, Anal. Chem. **80**, 1039–1048 (2008).
[43]R. Dhopeshwarkar, S. A. Li, and R. M. Crooks, Lab Chip **5**, 1148–1154 (2005).
[44]A. R. Khare and N. A. Peppas, Biomaterials **16**, 559–567 (1995).
[45]B. Yildiz, B. Isik, M. Kis, and O. Birgul, J. Appl. Polym. Sci. **88**, 2028–2031 (2003).
[46]S. J. Kim and J. Han, Anal. Chem. **80**, 3507–3511 (2008).
[47]A. Mani, T. A. Zangle, and J. G. Santiago, Langmuir **25**, 3898–3908 (2009).
[48]W. H. Smyrl and J. Newman, Trans. Faraday Soc. **63**, 207–216 (1967).
[49]V. G. Levich and D. B. Spalding, *Physicochemical Hydrodynamics: V. G. Levich Festschrift* (Advance Publications, 1977).
[50]I. Rubinstein and L. Shtilman, J. Chem. Soc., Faraday Trans. 2 **75**, 231–246 (1979).
[51]I. Rubinstein and B. Zaltzman, Phys. Rev. E **62**, 2238–2251 (2000).
[52]I. Rubinstein and B. Zaltzman, Math. Models Methods Appl. Sci. **11**, 263–300 (2001).
[53]B. Zaltzman and I. Rubinstein, J. Fluid Mech. **579**, 173–226 (2007).
[54]R. J. Hunter, *Zeta Potential in Colloid Science: Principles and Applications* (Academic Press, 1981).
[55]W. B. Russel, D. A. Saville, and W. R. Schowalter, *Colloidal Dispersions* (Cambridge University Press, 1992).
[56]J. H. Masliyah and S. Bhattacharjee, *Electrokinetic and Colloid Transport Phenomena* (Wiley, 2006).
[57]R. Das and G. H. Pollack, Langmuir **29**, 2651–2658 (2013).
[58]B. Chai, A. G. Mahtani, and G. H. Pollack, Contemp. Mater. **1**(3), 1–12 (2012).
[59]T. A. Zangle, A. Mani, and J. G. Santiago, Chem. Soc. Rev. **39**, 1014–1035 (2010).
[60]See supplementary material at http://dx.doi.org/10.1063/1.4939434 for a more detailed description of electrokinetic ICP demonstrations using an ionic hydrogel nanoporous network and videos.